Chemical Imaging of Surfaces with the Scanning Electrochemical Microscope

ALLEN J. BARD, FU-REN F. FAN, DAVID T. PIERCE, PATRICK R. UNWIN, DAVID O. WIPF, FEIMENG ZHOU

Scanning electrochemical microscopy is a scanning probe technique that is based on faradaic current changes as a small electrode is moved across the surface of a sample. The images obtained depend on the sample topography and surface reactivity. The response of the scanning electrochemical microscope is sensitive to the presence of conducting and electroactive species, which makes it useful for imaging heterogeneous surfaces. The principles and instrumentation used to obtain images and surface reaction-kinetic information are discussed, and examples of applications to the study of electrodes, minerals, and biological samples are given.

MOST MICROSCOPES OPERATE ON THE BASIS OF THE interaction of electromagnetic radiation with a sample to produce a two-dimensional (2-D) image. The appearance of the image is based on the relative absorbance (that is, the transparency), or, for opaque samples, reflectivity, of the sample components, with a resolution determined by the wavelength of the radiation used. In recent years new forms of microscopies, generally called scanning probe microscopies, have been introduced. These microscopies are based on scanning a small sharp tip in close proximity to a surface and recording the motion of the tip perpendicular to the surface (the z-direction) as it scans the x-y plane. The resulting image is a three-dimensional (3-D) display that is a function of the surface properties and topography of the sample. For example, the scanning tunneling microscope (STM) images by maintaining the tunneling current between the tip and a conducting or semiconducting sample constant (*1*), and the atomic force microscope (AFM) measures the force between tip and sample as a function of x-y position (*2*). The resolution of these techniques depends on the tip-sample spacing and the tip size; in favorable cases the STM and AFM can produce atomic resolution.

Our group has been developing a scanning probe microscope called the scanning electrochemical microscope (SECM), which is a "chemical microscope" that has a response based on mass transfer and chemical reactions at the scanning tip and the sample (*3*). Although the resolution of this technique, currently of the order of 100 nm, does not yet approach that of the STM and AFM, it is useful in obtaining topographic and chemical information about a wide range of sample surfaces, including electrodes, minerals, polymers, and biological materials. In this article we discuss the operating principles of the SECM and illustrate its application to a number of different samples, stressing recent applications. Earlier work with the SECM has recently been reviewed (*4, 5*).

The authors are in the Department of Chemistry and Biochemistry, University of Texas, Austin, TX 78712.

Basic Principles

A schematic diagram of the SECM is shown in Fig. 1. The tip and sample are immersed in a solution that contains an electroactive species, represented by Ox [for example, a metal complex like $Fe(CN)_6^{3-}$]. The tip is one electrode in an electrochemical cell that includes a reference electrode and an auxiliary electrode. The sample, if it is a conductor or semiconductor, can also be connected as an electrode in the cell, although frequently it is not. Insulators, including mineral and biological samples, are not part of the electrochemical cell circuit and are simply positioned beneath the tip.

To understand how the SECM operates, it is useful to review briefly the principles of electrochemical cells and the behavior of very small electrodes [so-called ultramicroelectrodes (UMEs)]. An UME is a conductive disk, frequently Pt, with a diameter of 0.1 to 25 μm, that is embedded in an insulating sheath. When the potential of the UME (also called "the tip") is adjusted by the external circuit (the bipotentiostat) with respect to the reference electrode to a sufficiently negative value, the species Ox is reduced at the disk surface in the electrode reaction $Ox + ne^- \rightarrow Red$ (Fig. 2A). This results in a current flow, i_T. The current is characterized by a transient, the duration of which depends on the UME disk diameter, that decays to a steady-state value, $i_{T,\infty}$. The steady-state current is governed by the mass transfer (flux) of Ox in solution to the UME, and is given by

$$i_{T,\infty} = 4nFCDa \quad (1)$$

where F is Faraday's constant, C is the concentration of Ox in solution, D is its diffusion coefficient, and a is the diameter of the UME disk.

Equation 1 holds when the UME is positioned "far" (that is, several disk diameters) away from a surface. When it is closer to a sample surface, the measured current is different from $i_{T,\infty}$. Near an insulator, the diffusion of Ox to the tip will be partially blocked, so that $i_T < i_{T,\infty}$ (Fig. 2B), approaching zero at very small separations. This decrease in current is called "negative feedback." On the other hand, when the tip is close to a conductive surface, the species produced at the tip surface, Red, can diffuse to the surface and be oxidized back to Ox (Fig. 2C). When this occurs, the flux of Ox to the tip is increased, and $i_T > i_{T,\infty}$. This is called "positive feedback." Thus, the ratio $i_T/i_{T,\infty}$ is a measure of the distance, d, between tip and substrate and an indicator of the nature (insulating or conducting) of the sample. Theoretical treatments are available for predicting this variation on the basis of, for example, computer simulations of the diffusion of Ox and Red in the gap between tip and sample (*6*), and general dimensionless plots of $i_T/i_{T,\infty}$ against a/d can be prepared for

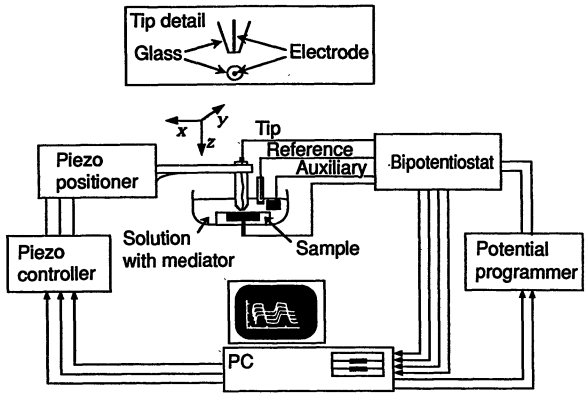

Fig. 1. Block diagram of the SECM.

determining d over either an insulator or conductor. Alternative theoretical treatments of the complete transient [$i_T(t)$] yield results for the steady-state current that are in good agreement with the original simulation (*7, 8*).

The UME tip is moved, with nanometer resolution, in the x-, y-, and z-directions by attached piezoelectric elements (Fig. 1), just as in the STM. These elements, as well as the bipotentiostat, are controlled by a personal computer, which records i_T as a function of tip position. The plot of i_T as a function of tip position in the x-y plane is the SECM image. This image can be converted to a plot of d versus x-y position or plotted as a gray-scale image, for example, where high values of i_T are shown as light colors and small values as dark colors. Images of many different types of samples, including electronically conducting polymers (*9*), leaves (*10*), metal electrodes (*11*), ionomeric polymers (*12*), and semiconductors (*13*) have been obtained with the SECM.

SECM Images

Different presentations of the SECM image of an interdigitated electrode array (IDA), which consists of Pt bands (3 μm wide and 0.1 μm thick) deposited on an SiO_2 substrate and spaced 5 μm apart, are shown in Fig. 3 (*14*). For this image a Pt disk (0.2 μm diameter) coated with glass served as the tip, and this tip and the IDA were immersed in a solution of 0.2 M $MVCl_2$ and 2 M KCl (MV^{2+} is methyl viologen dication). The tip was held at −0.76 V versus a saturated calomel reference electrode (SCE), where the reaction $MV^{2+} + e^- \rightarrow MV^+$ occurred. A single scan across the bands is shown in Fig. 3A. When the tip is over the insulating SiO_2, the current is much smaller than when it is over Pt, where positive feedback occurs, because the MV^+ produced at the tip is reoxidized to MV^{2+}. For this sample the changes in current do not represent topographical changes, but rather differences in the chemical nature (as reflected by the conductivity) of the surface. (We address the question of differentiating effects of topography and surface properties below.) A 3-D image is obtained by scanning in the x-y plane (Fig. 3B). This image can then be converted, if desired, to a gray-scale image, in which the light colors represent higher i_T values (Pt) and the darker colors represent the lower values (SiO_2) (Fig. 3C).

Two additional images are shown in Figs. 4 and 5. Figure 4 is an image of a single filament of blue-green algae (*Cyanobacterium oscillatoria*) collected from a local pond. The algae was mounted by placing it on a glass slide coated with a thin film of bovine serum albumin (BSA). Treatment of the slide with a 25% solution of glutaraldehyde in water cross-linked the BSA and formed a water-insoluble bond to the algae. What appear to be individual cells of the algae filament are apparent from the indentations that indicate the cell-wall junctions. The cell size indicated by SECM is consistent with that determined by optical microscopy. The morphology of the algae is also seen in the SECM image, with a prominent bulge in the center of each cell.

An SECM image of a silver filter membrane is shown in Fig. 5. The membrane (Selas-Flotronics, Spring House, Pennsylvania) is formed from small silver particles that have been sintered to form a porous film with an average pore size of ~5 μm. The SECM image was made under positive feedback conditions, indicating that the silver particles are electronically conducting.

The resolution attainable with the SECM is largely governed by the diameter of the scanning tip and the distance between tip and sample d, with a very small diameter tip moved in close proximity to the surface (that is, $d/a \approx 0.1$). For $a < 100$ nm, scanning at 10 nm above the surface and measuring the current becomes difficult, because stray vibrations and irregularities in the surface can cause a "tip crash." Thus, for high resolution the SECM must be operated in the constant current mode, as is often used with the STM, where d is adjusted by a feedback loop to the z-piezo to maintain i_T constant. This is straightforward when the sample is either all conductive or all insulating. However, for samples that contain both types of regions, a method of recognizing the nature of the substrate must be available. One approach is to modulate the motion of the tip in the z-direction and record the sign of di_T/dz (*15*), because i_T increases when the tip approaches a conductor but decreases when the tip approaches an insulator. Resolution can be improved (deblurred) by the use of image-processing techniques that remove the diffusional broadening by use of a Gaussian filter (*16*).

Imaging Surface Reactivity

The designations given above for samples as conductive and insulating actually represent limiting conditions and imply that the rate of mediator turnover (for example, Red → Ox + ne^-) at the sample surface is either very fast (diffusion controlled) or essentially zero, respectively. However, intermediate rates for the electron transfer (ET) reaction of the mediator are also possible. Under these conditions, the feedback current has a value between the two extremes and is a good predictor of the rate constant of the reaction, k, at the substrate surface. One area of interest is the examination of

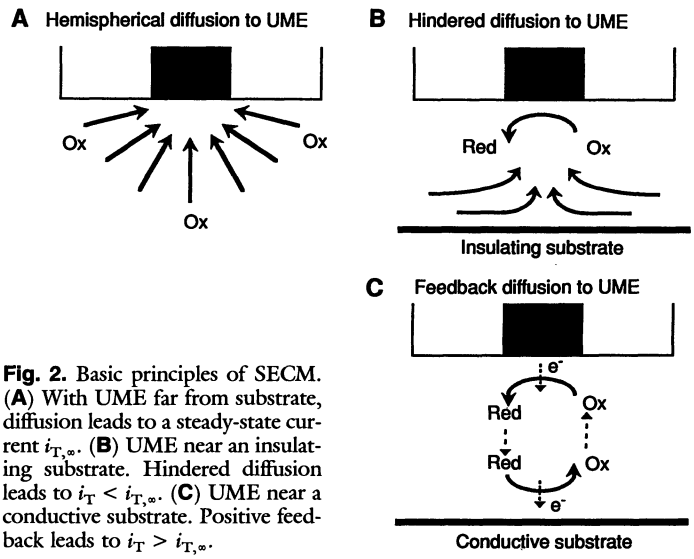

Fig. 2. Basic principles of SECM. (**A**) With UME far from substrate, diffusion leads to a steady-state current $i_{T,\infty}$. (**B**) UME near an insulating substrate. Hindered diffusion leads to $i_T < i_{T,\infty}$. (**C**) UME near a conductive substrate. Positive feedback leads to $i_T > i_{T,\infty}$.

electrode surfaces, where the rate of an electron transfer reaction is often a function of the nature of the electrode material. For example, the standard heterogeneous rate constant for the oxidation of Fe^{2+} to Fe^{3+} is fairly rapid on Pt or Au but is quite slow on carbon.

The sensitivity of the SECM feedback current to the substrate-mediator turnover rate suggests a new type of imaging process. With appropriate choice of mediator or substrate potential or both, it is possible to image variations in turnover activity, a technique we call reaction-rate imaging. At a conducting substrate, variations in the ET rate may arise because of the presence of catalytic particles or defect sites; alternatively, the electrode may be passivated by adsorbates or blocking layers. Reaction-rate imaging is demonstrated in Fig. 6. Here, the substrate is a composite electrode of Au regions embedded in a glassy carbon (GC) matrix. For the mediator solution used, Fe^{3+} ion in 1 M H_2SO_4, the Au regions are significantly more active than the GC regions. The SECM image in Fig. 6A was obtained when a Pt tip (10-μm diameter) was scanned over a 200-μm by 130-μm region of the composite, with the composite biased at +0.57 V versus the Fe(III)/Fe(II) formal potential (*17*). The bright regions represent the larger feedback currents over the Au regions and are due to the larger ET rate compared to the GC regions.

The rate is also a function of the electrode potential. If this potential is sufficiently positive, the oxidation of Fe^{2+} is rapid at GC. The image in Fig. 6B was scanned over the same region as that in Fig. 6A but with the composite biased at a potential of +0.82 V. In Fig. 6B the ET rates at both phases are at the diffusion limit, and a more uniform image results. However, only reaction rate differences are observed in the images, and topographic features are retained; for example, the round depression in the upper right of both images is due to a pit in the GC surface. Reaction-rate imaging should be useful in finding hot or catalytic sites on a surface or noting passivated areas, such as in studies of corrosion. The sensitivity of i_T to reaction rate can also be used in a more quantitative manner to determine the rate constant of the ET reaction, for example, from a plot of i_T versus d (*18*).

Kinetic Measurements and Imaging of Enzyme Sites

Reaction-rate imaging is not limited to studies of electrodes. In principle, any surface that has sufficient driving force to regenerate the mediator species consumed in the tip reaction can be studied. To this end, we have initiated studies of the redox reactions associated with surface-immobilized, as well as tissue-bound, enzymes. Our preliminary results indicate that with sufficient enzyme activities and surface densities the SECM feedback response can yield the same kind of heterogeneous rate information and active site images demonstrated above for electrodes.

The broad class of redox-active enzymes known as oxidoreductases have the most immediate application to the SECM experiment. In most of these systems, the enzyme catalyzes the transfer of electrons from an available redox mediator (Med) to a highly specific substrate molecule (Sub). If mediators are used that can be easily and reversibly changed from one redox form to another and if high substrate concentrations are used to keep the enzyme fully reduced or oxidized, the SECM can be used to probe both the kinetics and distribution of surface-constrained oxidoreductases (Fig. 7). The mediator generated at the SECM tip provides the reducing or oxidizing equivalents needed to initiate and maintain the enzyme-catalyzed reaction. Near the surface, the current generated by the tip reaction would reflect the rate at which the enzyme reacts with the mediator. High rates, which result from high enzyme activity or high surface coverage, would produce positive feedback currents, whereas low rates would yield negative feedback, characteristic of insulating surfaces. The following examples demonstrate the use of such SECM responses, both for evaluating the kinetics associated with micrometer-scale regions of surface-constrained enzymes and for imaging biological samples with widely dispersed enzyme sites.

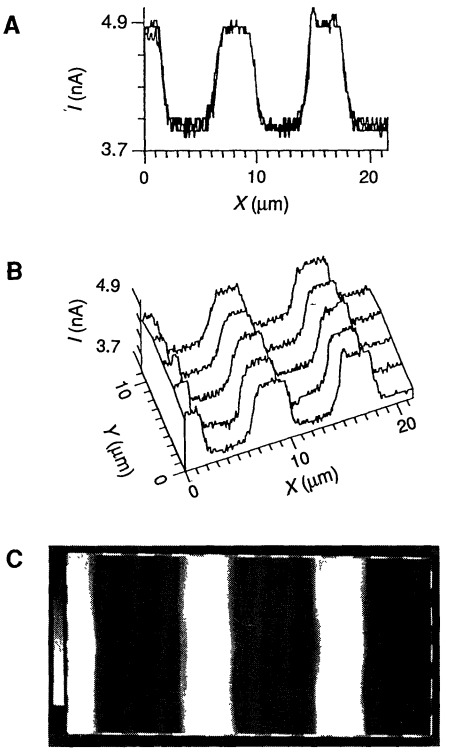

Fig. 3. Three presentations of the SECM image of an IDA (see text). (**A**) Single scan. (**B**) Three-dimensional view. (**C**) Gray-scale image ($i_{T,\infty}$ = 3.7 nA).

One of the bioenzyme systems chosen for study was that of glucose oxidase (GO). This enzyme, from the mold *Aspergillus niger*, has received considerable attention for its use in glucose biosensors (*19, 20*); its immobilization on electrodes and other surfaces has been examined extensively (*21*). Both immobilized and in solution, GO catalyzes the highly specific oxidation of β-D-glucose to δ-gluconolactone in the presence of a number of electron-accepting mediators (Med^{Ox}).

$$\beta\text{-D-glucose} + GO^{ox} \rightarrow \delta\text{-gluconolactone} + GO^{Red} \quad (2)$$

$$GO^{Red} + 2Med^{Ox} \xrightarrow{k_f} GO^{Ox} + 2Med^{Red} + 2H^+ \quad (3)$$

The SECM has been used with the configuration shown in Fig. 7A

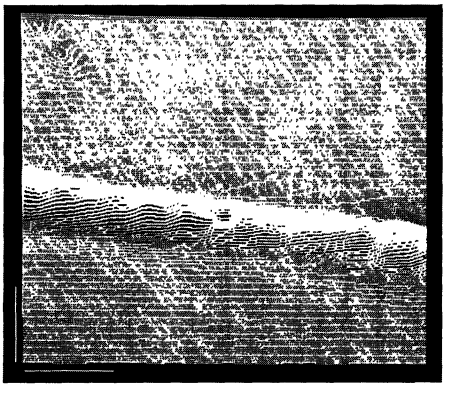

Fig. 4. SECM image of a filament of a blue-green algae (*C. oscillatoria*). The scan range is 49 μm by 49 μm. The mediator solution was a 2 mM solution of $Ru(NH_3)_6^{3+}$ in a phosphate-citrate buffer (pH 7.3, 0.05 M ionic strength). The tip was a Pt microdisk (1-μm radius) held at −0.23 V versus the mediator formal potential. The tip raster scan rate was 10 μm/s. Scale bars = 10 μm.

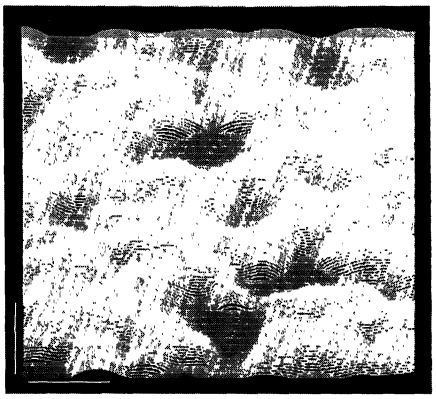

Fig. 5. SECM image of a silver filter membrane. The scan size is 45 μm by 45 μm. The image has been processed to convert the original current image into an absolute distance scale. The vertical scale is the tip-sample distance and ranges from 1 to 6 μm. The mediator solution was a 2.1 mM solution of ferrocene in 0.1 M tetra-*n*-butlyammonium tetrafluoroborate-acetonitrile. The tip was a Pt microdisk (1-μm radius) held at +0.3 V versus the mediator formal potential. The tip raster scan rate was 10 μm/s. Scale bars = 10 μm.

to measure the enzyme-mediator kinetics (Eq. 3) for GO immobilized on insulating materials (*22*). The current response of the mediator, ferrocenecarboxylic acid, at various distances from a nylon surface bound with GO is shown in Fig. 8. The increase in normalized current (under the conditions for the upper curve) reflected a finite contribution of the GO surface reaction to mediator turnover, and comparison to theory (*23*) yielded a rate constant of $k_f = (1.9 \pm 0.4) \times 10^{-3}$ cm s^{-1}. These findings demonstrate the ability of the SECM to measure enzyme kinetics under physiological conditions and over much smaller surface regions than those that have typically been possible.

We demonstrate reaction-rate imaging with mitochondria; their small size (0.5 to 3 μm) but highly active redox pathways provide a challenging and interesting substrate. Successful imaging depends on a judicious choice of the enzyme-substrate system. Low sensitivities can arise from slow cross-membrane diffusion or complete membrane impermeability of particular redox mediators. Only enzymes located on membranes or tissue structures directly exposed to the mediator solution can be directly probed by SECM. One of the nicotinamide adenine dinucleotide (NAD)–linked reductases located on the outer membrane of rat liver mitochondria is the rotenone-insensitive reduced NAD (NADH)–cytochrome b_5 reductase (NR) (*24*). This enzyme catalyzes the rapid reduction of various exogenous mediators in the presence of high concentrations of β-NADH (*25, 26*) and was utilized for the SECM imaging of glass-immobilized rat liver mitochondria (Fig. 7B).

With tetramethyl-*p*-phenylenediamine (TMPD) acting as mediator and with a tip height of ~3 μm, rastered SECM images of the feedback current were obtained over regions containing moderate densities of whole mitochondria (*22*) (Fig. 9). Over glass regions, the images were quite flat, with the small i_T indicative of negative feedback caused by the insulating surface. Over immobilized mitochondria, the images were somewhat blurred because of the large size of the carbon fiber tip (8-μm diameter) relative to mitochondrial dimensions. The decreased current response at the perimeter of each mitochondrion (maximum dimensions ~20 μm) was indicative of the surface relief of these organelles, which partially blocked the radial diffusion of mediator to the carbon fiber tip. Only when the fiber was very near a particular mitochondrion did the NR-TMPD surface reaction augment mediator turnover and cause a small rise in current (mean dimensions of about 4 μm by 8 μm). Because this increase in the SECM response was not observed in the absence of NADH, Fig. 9 reflects discrimination of enzyme activity at the micron level.

Dynamic and Equilibrium Measurements at Insulator Surfaces

The SECM is also a useful tool for studying solid-liquid interfacial processes such as adsorption-desorption or dissolution at high spatial resolution. Such processes are of fundamental importance in a variety of areas in the physical and biological sciences. However, a lack of suitable experimental methodology has severely limited dynamic studies on insulating materials of the elementary steps in these processes (*27, 28*). SECM-induced desorption (SECMID) is a new approach for studying this class of reaction, and this approach provides the first opportunity to measure rapid adsorption-desorption processes of electroactive adsorbates at well-defined (for example, single-crystal) surfaces.

In this case dynamic studies are carried out by measuring transients, that is, i_T versus time, with the tip held at a given distance d over a given spot on the substrate. The principles of SECMID are illustrated schematically in Fig. 10 with the TiO_2/H^+ system as an example; surface acidity is a significant field in solid-liquid interfacial adsorption (*29–32*). A potential step is applied to the tip electrode,

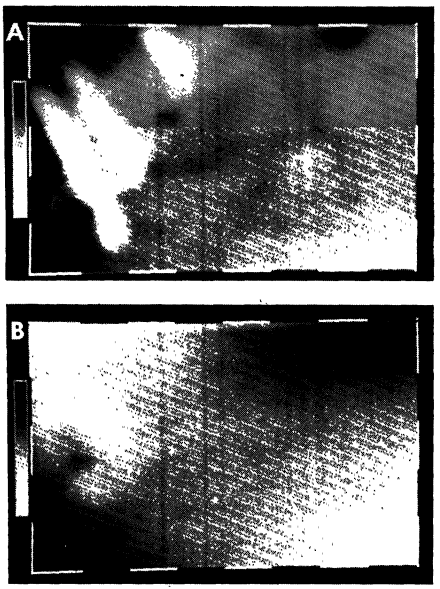

Fig. 6. Gray-scale images of a composite GC/Au surface. The mediator is 2.0 mM Fe(III) in 1 M H_2SO_4. The tip is a Pt disk (10-μm diameter) held at −0.47 V, where the reaction $Fe^{3+} + e^- \rightarrow Fe^{2+}$ occurs; tip scan speed is 10 μm/s. Potentials are versus the Fe^{3+}/Fe^{2+} formal potential. Imaged region is 200 μm by 130 μm. (**A**) Substrate potential of +0.57 V; current scale 2.8 to 4.3 nA. (**B**) Substrate potential of +0.82 V; current scale 5.5 to 7.6 nA. Scale bars = 25 μm.

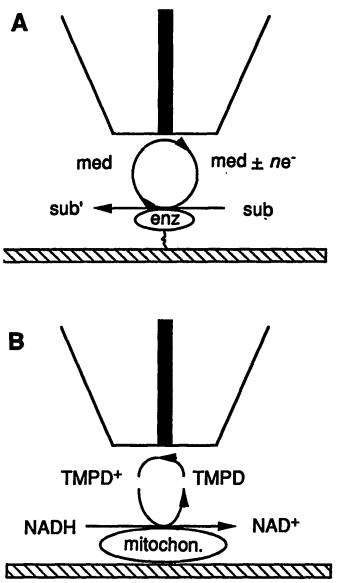

Fig. 7. Schemes depicting the principles of positive-feedback detection of enzymes: (**A**) SECM tip near a surface-constrained enzyme (enz) with mediator (med) turnover generated in the presence of substrate (sub); (**B**) SECM tip imaging of a single mitochondrion (mitochon.) through the use of the outer membrane enzyme, NADH–cytochrome b_5 reductase.

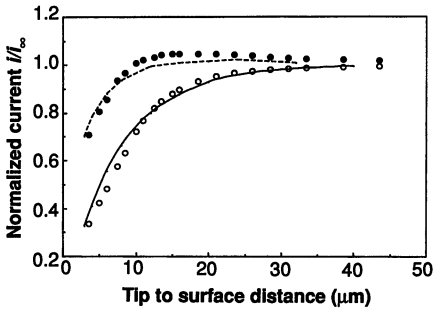

Fig. 8. SECM tip current versus distance characteristics for the mediator, 0.52 mM ferrocenecarboxylic acid (D = 6.4 × 10^{-6} cm^2 s^{-1}), in 0.1 M phosphate buffer (pH 7.0) near a nylon surface bound with glucose oxidase. The tip is a carbon fiber (8-μm diameter) held at a potential of +0.6 V versus SCE. The lower points (open circles) correspond to a solution without D-glucose present, and the upper points (filled circles) correspond to a solution with [D-glucose] = 50 mM. Lines represent the theoretical behavior for an irreversible surface reaction with rate constants of k_f = 0 cm s^{-1} (solid line) and k_f = 1.89 × 10^{-3} cm s^{-1} (dashed line).

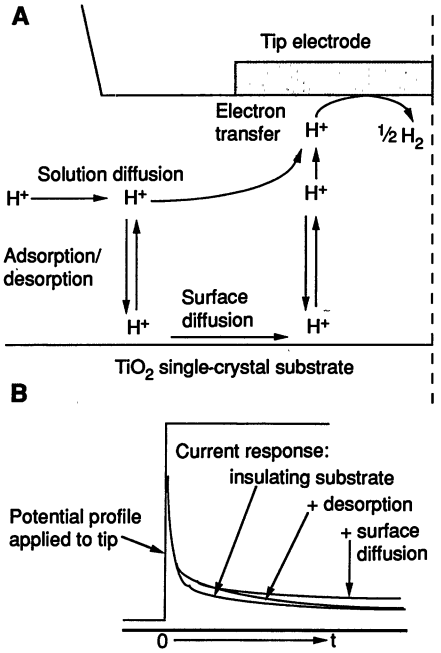

Fig. 10. Principles of SECMID, showing schematically (**A**) transport processes in the tip-substrate domain and (**B**) the potential profile applied to the tip electrode and the possible current responses.

which is positioned above the substrate, such that the electrolysis of the solution component of the adsorbate (reduction of H^+ to H_2 in the example) is diffusion-controlled. The consequent decrease in the concentration of H^+ in the tip-substrate domain both perturbs the adsorption-desorption equilibrium, which induces the desorption of H^+ from the TiO_2 surface, and promotes the diffusion of H^+ through solution into the gap region. Moreover, because the desorption process depletes the concentration of H^+ on the substrate directly under the tip, surface diffusion can also provide a path for the transport of H^+ into the gap domain. The flux of protons at the tip electrode, and hence the current-time behavior, is a measure of the rates of these three processes.

Numerical models for SECMID have recently been developed (*33*). In the short-time region the desorption process provides an additional source of H^+ for electrolysis, and consequently the tip current is larger than that for an inert insulating substrate (Fig. 10B). The current becomes increasingly sensitive to this process as the tip-substrate separation is minimized, because this both hinders diffusion into the gap and maximizes the ratio of substrate surface area to solution volume in the tip-substrate domain. In the absence of surface diffusion the steady-state current attains the value for an inert insulating substrate; the adsorption-desorption system reaches a new equilibrium (governed by the local concentration of H^+ adjacent to the substrate interface), and the tip current depends only on diffusion of H^+ through solution. If the surface diffusion pathway operates to a significant extent, this can be detected through an increase in the steady-state current (*33*).

A typical experimental transient (displayed as normalized i_T versus $t^{-1/2}$) for the H^+/TiO_2 [rutile (001) surface] system, with a bulk concentration $[H^+]^*$ = 2 × 10^{-4} M, is shown in Fig. 11. This figure shows an increase in current in the short-time region, as compared to an inert insulator, that is diagnostic of desorption of H^+ from the TiO_2 interface. One can treat this process theoretically to obtain the adsorption and desorption rate constants, k_a and k_d, taking account of the change in surface charge density, and thus surface potential, during these processes (*33*). Complementary steady-state current-distance measurements for this system were as predicted for an inert insulator, suggesting that surface diffusion of H^+ at the TiO_2 interface is negligible.

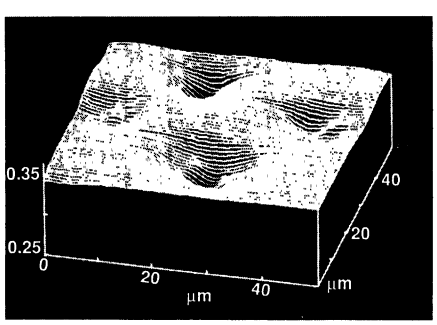

Fig. 9. SECM line-scan image of enzymatically active rat liver mitochondria immobilized on glass with the surface bathed in a 50-mM phosphate-buffered solution (pH 7.5) containing 0.25 M sucrose, 0.1 M KCl, 2 μM rotenone, and 50 mM β-NADH. The mediator, 0.9 mM TMPD, is oxidized at the carbon fiber tip (8-μm diameter) at a potential of +0.2 V versus SCE. Vertical axis is $i_T/i_{T,\infty}$.

In addition to dynamic studies, the SECM can also be used to measure adsorption isotherms. Experiments of this nature use the tip electrode to amperometrically monitor the concentration of electroactive adsorbate remaining in a small drop of solution (typically 10 to 20 μl), c^*_d, deposited on the surface (typically covering an area of 0.15 to 0.30 cm^2). This new method provides a high ratio of surface area to solution volume required for analytical sensitivity while allowing the use of well-defined (for example, single crystal) surfaces. The value of c^*_d is obtained directly from the diffusion-limited current at the tip, Eq. 1, with $C = c^*_d$. The concentration of solute in the absence of adsorption, c^*_s, can similarly be determined electrochemically, and the difference in limiting currents used to calculate the concentration of material adsorbed at the interface (in moles per square centimeter) is as follows:

$$\Gamma_{ad} = (V/A)\,(i_s - i_d)/(4nFDa) \quad (4)$$

where i_s is the measured current in the absence of adsorption, V is the drop volume, and A the area of the substrate that it covers.

This approach was applied to study the adsorption of H^+ on the {010} surface of the mineral albite ($NaAlSi_3O_8$), which undergoes protonation (solution pH < 7) and deprotonation (pH > 7) of surface hydroxyl groups in addition to rapid exchange of H^+ for Na^+ in the absence of Na^+ in solution (*34*). Through judicious selection of the surface pretreatment of albite, it has been possible to measure the isotherm for the protonation of –OH groups and estimate the number of protonation and exchange sites (*35*).

Studies of Homogeneous Kinetics

The SECM can also be used to study the rate of homogeneous chemical reactions of species generated at the tip as they traverse the

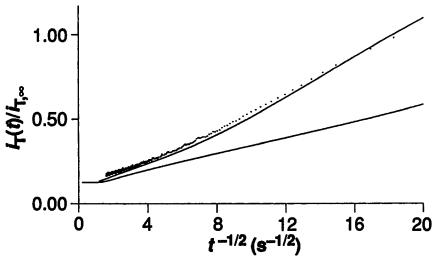

Fig. 11. Current-time characteristics for the reduction of 2 × 10^{-4} M H^+ at a Pt tip electrode (25-μm diameter) held 2.6 μm above a TiO_2 (001) substrate. The lower solid line corresponds to the behavior predicted for an inert insulating substrate, and the upper solid line is the best theoretical fit to the data (*33*).

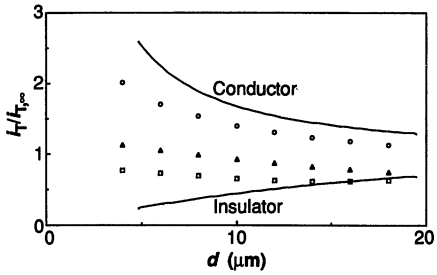

Fig. 12. SECM steady-state $i_T - d$ characteristics for the oxidation of DMPPD (5 × 10^{-4} M) at pH 10.20 (○), 10.78 (▲), and 11.24 (□), with an unbiased platinum substrate. The solid lines represent theoretical behavior in the absence of coupled reaction for insulating and conductive substrates. [Reprinted from (*8*) with permission, © 1991 American Chemical Society]

solution gap to a conductive substrate. In this application the tip-substrate electrode pair is somewhat analogous to the disk and ring electrodes in the rotating ring-disk electrode (*36*) or the walls of a thin-layer electrochemical cell (*37*). Consider again the situation of Fig. 2C. The magnitude of the positive feedback current depends on the tip-generated species, Red, traversing the solution gap by diffusion and being oxidized to Ox at the conductive substrate. If species Red undergoes some reaction to form a nonelectroactive species during this time, i_T would be decreased, because mediator is being removed from the gap region by the reaction. Thus, measurement of i_T versus d and a comparison to the unperturbed positive feedback response can yield the rate constant, k, for the decomposition of Red. An estimate of the range of accessible rate constants can be obtained by a comparison of the time for Red to traverse the gap, τ, ($\sim d^2/D$) and the lifetime of Red ($\sim 1/k$ for a first-order reaction and $\sim 1/kC$ for a second-order reaction). Thus, useful dimensionless parameters are d^2k/D or d^2kC/D for first- and second-order reactions, respectively. If the parameter is much larger than 1, Red would disappear in the gap, and insulating behavior would be observed. If it is much smaller than 1, there is no effect of the reaction, and conductive behavior would result. Useful measurements can be made when the parameter is of the order of 1, that is, when $k \approx D/d^2$ or D/d^2C. For example, if a measurement can be made at a d of 0.1 μm, a first-order k of about 10^5 s^{-1} should be accessible. At d = 100 Å, which is probably the closest practical approach before tunneling effects become possible, a k of 10^7 s^{-1} could be measured.

A theoretical treatment for a first-order reaction, along with an experimental study of the oxidation of *N,N*-dimethyl-*p*-phenylenediamine (DMPPD) in aqueous solutions with the SECM has appeared (*8*). The reactions of interest are the following:

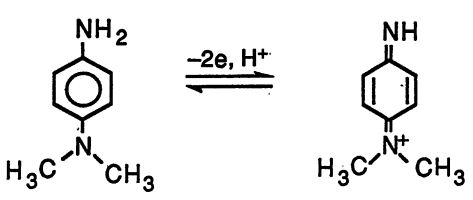

(I) (II) (5)

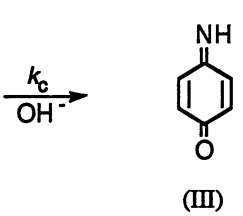

(III) (6)

with DMPPD oxidized at the tip. From plots of $i_T/i_{T,\infty}$ versus d (Fig. 12), a rate constant for the reaction in Eq. 6 of about 10^4[OH^-] M^{-1} s^{-1} over a pH range of 10.2 to 11.2 was obtained. Kinetic measurements on the SECM can also be carried out by transient methods (*8*). The same approach has been used for a second-order reaction, the coupling of dimethylfumarate radical anions after generation at a tip in a *N,N*-dimethylformamide solution (*38*).

Conclusions

Although the SECM is a recently developed instrument, it has already found use in the characterization of a number of different types of surfaces and for the study of different types of chemical and physical processes. Other applications are possible, including characterization of the processes that occur in polymer layers on surfaces (*39*) and the characterization of membranes (*40*). The SECM is also a useful tool for high-resolution modification and fabrication of structures on surfaces (*4, 41–45*). For example, the SECM can be used to deposit metal lines as narrow as 0.3 μm and etch lines or holes in metals and semiconductors. Higher resolution with the SECM depends on the ability to construct smaller insulated tips with the proper geometry and the ability to scan close to the substrate in the constant-current mode. Although atomic resolution cannot be attained with the SECM because tunneling effects dominate at distances needed for such resolution (~10 Å), we believe that an ultimate resolution of several hundred angstroms is possible.

REFERENCES AND NOTES

1. G. Binnig and H. Rohrer, *Helv. Phys. Acta* **55**, 726 (1982).
2. G. Binnig, C. Quate, C. Gerber, *Phys. Rev. Lett.* **56**, 930 (1986).
3. A. J. Bard, F.-R. F. Fan, J. Kwak, O. Lev, *Anal. Chem.* **61**, 132 (1989).
4. A. J. Bard, G. Denuault, C. Lee, D. Mandler, D. O. Wipf, *Acc. Chem. Res.* **23**, 357 (1990).
5. R. C. Engstrom and C. M. Pharr, *Anal. Chem.* **61**, 1099A (1989).
6. J. Kwak and A. J. Bard, *ibid.*, p. 1221.
7. M. V. Mirkin and A. J. Bard, *J. Electroanal. Chem.*, in press.
8. P. R. Unwin and A. J. Bard, *J. Phys. Chem.*, in press.
9. J. Kwak, C. Lee, A. J. Bard, *J. Electrochem. Soc.* **137**, 1481 (1990).
10. C. Lee, J. Kwak, A. J. Bard, *Proc. Natl. Acad. Sci. U.S.A.* **87**, 1740 (1990).
11. J. Kwak and A. J. Bard, *Anal. Chem.* **61**, 1794 (1989).
12. C. Lee and A. J. Bard, *ibid.* **62**, 1906 (1990).
13. D. Mandler and A. J. Bard, *Langmuir* **6**, 1489 (1990).
14. C. Lee, C. J. Miller, A. J. Bard, *Anal. Chem.* **63**, 78 (1991).
15. D. O. Wipf and A. J. Bard, in preparation.
16. C. Lee, D. O. Wipf, A. J. Bard, K. Bartels, A. Bovik, *Anal. Chem.*, in press.
17. D. O. Wipf and A. J. Bard, *J. Electrochem. Soc.* **138**, L4 (1991).
18. ———, *ibid.*, p. 469.
19. A. Heller, *Acc. Chem. Res.* **23**, 128 (1990).
20. A. P. F. Turner, I. Karule, G. S. Wilson, Eds., *Biosensors: Fundamentals and Applications* (Oxford Univ. Press, Oxford, 1987).
21. D. L. Wise, Ed., *Bioinstrumentation and Biosensors* (Dekker, New York, 1991).
22. D. T. Pierce, P. R. Unwin, A. J. Bard, in preparation.
23. A. J. Bard, M. Mirkin, P. R. Unwin, D. O. Wipf, in preparation.
24. G. L. Sottocasa, L. E. Kuylenstierna, A. Bergstrand, *J. Cell Biol.* **32**, 415 (1967).
25. P. Bernardi and G. F. Azzone, *Biochim. Biophys. Acta* **679**, 19 (1982).
26. M. Wikstrom and R. Casey, *FEBS Lett.* **183**, 293 (1985).
27. M. Anderson, C. Bauer, D. Hansmann, N. Loux, R. Stanforth, in *Adsorption of Inorganics at Solid-Liquid Interfaces*, M. A. Anderson and A. J. Rubin, Eds. (Ann Arbor Science, Ann Arbor, MI, 1981), pp. 327–347.
28. K. Hachiya, K. Takeda, T. Yasunaga, *Adsorpt. Sci. Technol.* **4**, 25 (1987).
29. C. P. Huang, in *Adsorption of Inorganics at Solid-Liquid Interfaces*, M. A. Anderson

and A. J. Rubin, Eds. (Ann Arbor Science, Ann Arbor, MI, 1981), pp. 183–217.
30. R. O. James, in *ibid.*, pp. 219–261.
31. P. W. Schindler and W. Stumm, in *Aquatic Surface Chemistry*, W. Stumm, Ed. (Wiley, New York, 1987), pp. 83–110.
32. D. A. Dzombak and F. M. M. Morel, *Surface Complexation Modelling* (Wiley, New York, 1990).
33. P. R. Unwin and A. J. Bard, in preparation.
34. A. Blum and A. Lasaga, *Nature* **331**, 431 (1988).
35. P. R. Unwin and A. J. Bard, in preparation.
36. W. J. Albery and M. L. Hitchman, *Ring-Disc Electrodes* (Clarendon, Oxford, 1971).
37. A. T. Hubbard and F. C. Anson, in *Electroanalytical Chemistry*, A. J. Bard, Ed. (Dekker, New York, 1970), vol. 4, p. 129.
38. F. Zhou, P. R. Unwin, A. J. Bard, unpublished results.
39. J. Kwak, C. Lee, F. Anson, personal communication.
40. E. R. Scott, H. S. White, J. B. Phipps, *J. Membr. Sci.* **58**, 71 (1991).
41. O. E. Hüsser, D. H. Craston, A. J. Bard, *J. Vac. Sci. Technol. B* **6**, 1873 (1988).
42. Y.-M. Wuu, F.-R. F. Fan, A. J. Bard, *J. Electrochem. Soc.* **136**, 885 (1989).
43. D. Mandler and A. J. Bard, *ibid.*, p. 3143.
44. ———, *ibid.* **137**, 1079 (1990).
45. ———, *ibid.*, p. 2468.
46. The support of this research by grants from the Robert A. Welch Foundation, the Texas Advanced Research Program, and the NSF is gratefully acknowledged. P.R.U. thanks SERC for the award of a NATO fellowship. We thank D. M. Zeigler for providing the mitochondria used in this work.

Chemical Microsensors

R. C. HUGHES, A. J. RICCO, M. A. BUTLER, S. J. MARTIN

Recent developments in the field of chemical microsensors are leading to new applications for which these devices have the potential to supplement or replace traditional analytical chemical instrumentation. The fundamentals of current microelectronic, acoustic wave, optical fiber, and electrochemical microsensors are presented, and a few recent, exciting results in these areas are described. Although future opportunities in the microsensor field are numerous, many significant problems, the majority of them related to the materials utilized for the chemically sensitive layers that are the "front end" of these devices, remain to be explored and solved.

MANY TASKS FACED BY MODERN ANALYTICAL CHEMISTRY are difficult to solve with conventional, laboratory-based analytical instruments for reasons of size, speed, or cost. The chemical microsensor finds its niche when a continuous measurement of a chemical concentration is required from a number of locations, and only a small space or low power (or both) are available for each sensor. As a result of interest in such potential applications, many researchers are active in this field, and a great deal of literature exists (*1–4*).

Some of the applications that have been cited by existing or potential users of microsensors who believe that existing instrumentation is inadequate are listed in Table 1. Many such applications arise because time does not permit obtaining a sample and returning it from the field to the laboratory. Furthermore, in many cases it is unnecessary to have a detailed chemical analysis of each sample: only the concentration is of interest because the chemical species is already known for a particular site. In such cases, an inexpensive, nonselective microsensor may be the ideal solution.

As a result of the roots of microsensors in microelectronic mass production technology, the incremental cost of microsensors can be quite low. In contrast, the cost of chemical monitoring with conventional laboratory apparatus can be relatively high. An example is the analysis of a single sample from a well for monitoring ground-water contamination: the cost can exceed $300 by the time the sample is collected, transported to an analytical laboratory, and analyzed. In addition, such an analysis only gives one concentration data point in time and space, with the chance that the removal and transportation of the sample may have altered its chemical composition.

The authors are with the Microsensor Division, Sandia National Laboratories, Albuquerque, NM 87185.

In addition to the advantages of real-time, in situ, low-cost monitoring, chemical microsensors can, in some instances, provide very high sensitivity. The "micro" in microsensor becomes very important if the limits of sensitivity depend on the absolute number of molecules to be detected. An example is when a fixed, small volume sample (for example, the contents of a living cell) is all that is available, and essentially all of the desired species can be delivered to the microsensor. The response of chemical microsensors usually depends on the number of interacting molecules per unit area; thus, the smaller the device, the fewer molecules can be detected. In some instances, however, the limiting sensitivity may be related to the concentration of the species to be detected, in which case the size of the device has little effect on sensitivity. An example of this is monitoring a low concentration but essentially unlimited volume sample, such as an underground aquifer or a region of the atmosphere. Knowledge of the nature and extent of the sample is thus important in determining whether a microsensor can provide a sensitivity advantage. These concepts may falter for ultrasmall (submicrometer) sensor structures, in which the size of the sensing structure becomes comparable to the size or diffusion lengths (or both) of the molecules being detected.

The interface between the physical transducer and the chemical transducer can be complex. Thus, predicting the performance of a sensor often requires detailed knowledge not only of the device physics and the chemistry of the sensing layer, but of the interplay between the two as well. Although the principles of operation of the micro- and optoelectronic devices that serve as platforms for chemical microsensors are often well known to physicists and electrical engineers, chemical transducer coatings are alien to the world of microelectronics. Indeed, billions of dollars have been spent to stabilize microelectronic devices against the changes caused by chemical reactions. For example, electrically mobile sodium and